

SEMESTER THESIS

Design and coupling of a 3D microwave cavity to a waveguide

Author:
Maud BARTHÉLEMY

Supervisor:
Philipp KURPIERS

Professor:
Andreas WALLRAFF

September 29, 2014

EIDGENÖSSISCHE TECHNISCHE HOCHSCHULE ZÜRICH
SWISS FEDERAL INSTITUTE OF TECHNOLOGY ZURICH

ETH zürich

Abstract

A 3D microwave cavity can contain an electromagnetic field inside its walls. To transmit the information contained in the cavity, it is possible to couple it to a waveguide, e.g. through a hole in one of its wall. In this thesis, the design and fabrication of a cavity to fulfill specific requirements of the electromagnetic modes are realised. The coupling of the cavity to a waveguide is studied by simulations and by reflection measurements. The influence of different characteristics of the system on the coupling is investigated, such as the thickness of the wall between the cavity and the waveguide, the radius of the coupling hole and the quality of the material used. Good agreement is found between the simulations and the measurement results.

Contents

1	Introduction	1
2	Theory	2
2.1	Waveguide	2
2.2	3D cavity	3
2.3	S-parameters	3
2.4	Q-factor	4
3	Design of the cavity	5
3.1	Simulations	5
3.1.1	Cavity for the final system	5
3.1.2	Cavity for the study of the coupling	7
3.2	Design and fabrication of the cavity	8
4	Measurements	9
4.1	Measurement setup	9
4.2	Calibration and background subtraction	9
4.3	Measurement results	9
4.4	Fitting of the data	10
5	Results and discussion	13
5.1	Measurement results and discussion	13
5.2	Simulations and sources of errors	14
5.3	Measurements with high purity Aluminium	16
6	Conclusion	22
7	Acknowledgement	23

1 Introduction

The motivation for this project is the realisation of a system capable of measuring the violation of Bell's inequality, in which the detection and locality loophole are simultaneously closed.

Several experiments have been performed already to verify the violation of these inequalities [1] [2] [3]. The first experiment was realised using photons [4], then the most notable experiments were realised by Aspect et al. [5] [6]. However, two loopholes were left open.

First, the detection loophole, arising from the low detection efficiency of photon detectors : only a small portion of photons of all emitted photons are detected, with the possibility that the sub-ensemble of photons which are detected doesn't represent the whole ensemble. This lead to the 'fair sampling hypothesis', affirming that the sample of photons detected represent fairly the ensemble of whole photons emitted.

The second loophole is the locality (or lightcone) loophole. It relies on the fact that the duration of measurement is too long and the distance between the two particles too small, so that information could be transmitted between the two particles at velocity up to the speed of light.

The first experiment to overcome the locality loophole was realised in 1998 by Weihs et al. [8]. The detection of the photons were realised 400 m apart and the measurement of the order of the ns, so that no information could possibly be sent between the two detectors before the end of the measurements on both sides.

The detection loophole was closed for the first time in 2001, in an experiment by Rowe et al. [7] using ions. No fair-sampling hypothesis was required, as the outcome of every experiment was measured with sufficient fidelity.

Many experiments have been performed with various systems of photons, ions, neutrons [9] and even in solid state [10]. However, so far no experiment was performed completely loophole-free, such that local realistic theories cannot yet be ruled out.

The final system should be composed of two cavities connected by a several meters long waveguide, with a qubit positioned in the middle of each cavity. Read out will be performed by two coaxial cables on each cavity. To entangle the two qubits, the coupling between the cavity and the waveguide is a crucial characteristic to understand and realise such a system. This coupling, more specifically the coupling between the cavity and the waveguide, is the main focus of this report. The system is schematically illustrated in figure 1.

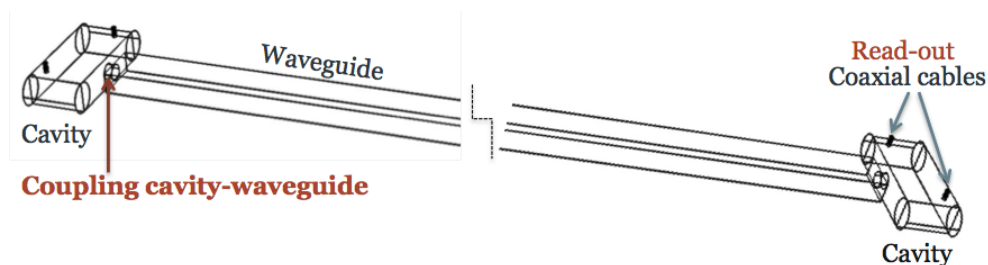


Figure 1: Sketch of the system

2 Theory

This chapter presents a theoretical background on waveguides and cavities. The characterisation of a system by the S-parameters and the Q-factor is also explained.

2.1 Waveguide

A waveguide is a hollow metallic structure guiding high frequency radio waves. The geometry of a rectangular waveguide is presented in figure 2. It is characterised by the two dimensions a and b of the waveguide, and by the permeability μ and permittivity ϵ of the material inside the waveguide.

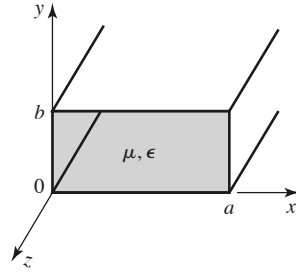


Figure 2: Geometry of a rectangular waveguide [12].

There are transverse electric (TE) and transverse magnetic (TM) modes. TE modes are modes with the component of the electric field along z , E_z , equal to zero and the component of the magnetic field along z , H_z , not equal to zero. TM modes are modes with $H_z = 0$ and $E_z \neq 0$. Both TE and TM modes can propagate in the waveguide. There is a cutoff frequency below which no mode can propagate.

The focus of this thesis is on TE modes. Each mode mn has a cutoff frequency f_c^{mn} given by :

$$f_c^{mn} = \frac{k_c}{2\pi\sqrt{\mu\epsilon}} \quad (2.1)$$

where the cutoff wavenumber k_c^{mn} can be written as :

$$k_c^{mn} = \sqrt{\left(\frac{m\pi}{a}\right)^2 + \left(\frac{n\pi}{b}\right)^2} \quad (2.2)$$

The dominant mode is the mode with the lowest cutoff frequency. For a rectangular waveguide, the dominant mode is the TE_{10} mode ($m = 1, n = 0$), with $f_c = \frac{1}{2a\sqrt{\mu\epsilon}}$. Usually only the dominant mode is interesting for propagation. This requires that the frequency range stays between the cutoff frequency of the TE_{10} mode and the cutoff frequency of the next mode.

For the waveguide WR90 with dimensions $a = 22.86$ mm and $b = 10.16$ mm, the recommended frequency band of operation is : 8.20 to 12.40 GHz (X-band), and the lower cutoff frequency $f_c = 6.56$ GHz. Figure 3 shows the ideal loss as a function of frequency for a WR90 waveguide made of copper. For frequencies below the cutoff frequency, there is no propagation in the waveguide, which corresponds to infinite loss. Then the loss drops after the cutoff frequency and stays really low in the operating frequency range.

Waveguides have a low bandwidth of operation, but their losses are also really low. For the WR90, at selected mid-band frequency, i.e. 10 GHz, the (ideal) loss if $\alpha = 0.108$ dB/m.

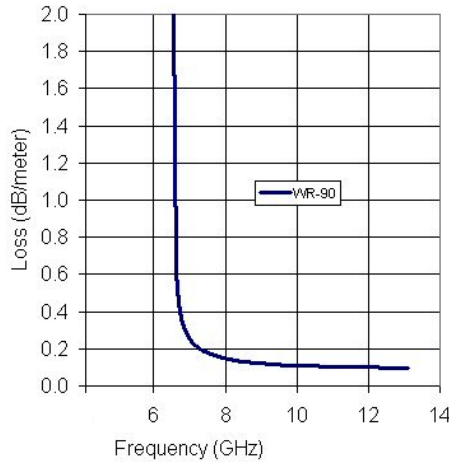


Figure 3: Waveguide loss for a WR90 out of copper. [13]

2.2 3D cavity

A cavity is a waveguide closed at both end, forming a closed box. The electric and magnetic energies are stored within the cavity. Power dissipation occurs in the metallic walls of the cavity and in the dielectric material filling the cavity. It is possible to realise a coupling by a small hole or a small probe in the cavity.

The propagation constant of the mn th TE or TM mode is $\beta_{mn} = \sqrt{k^2 - (\frac{m\pi}{a})^2 - (\frac{n\pi}{b})^2}$ where $k = \omega\sqrt{\mu\epsilon}$.

The solution is then given by : $\beta_{mnl}d = l\pi$ with $l = 1, 2, 3, \dots$, which implies that the cavity must be an integer multiple of a half-guide wavelength long at the resonant frequency.

The resonance wave number for the rectangular cavity can be defined as

$$k_{mnl} = \sqrt{\left(\frac{m\pi}{a}\right)^2 + \left(\frac{n\pi}{b}\right)^2 + \left(\frac{l\pi}{d}\right)^2} \quad (2.3)$$

2.3 S-parameters

The S-parameters represent the reflection and transmission coefficients in a system. They are the elements of the scattering matrix S. The S-parameters are complex number, with an amplitude and a phase, $S_{ij} \in \mathbb{C}$, where i indicates the output port and j the input port.

For $i = j$, S_{ii} is the reflection coefficient ; whereas for two different ports i and j ($i \neq j$), S_{ij} is the transmission coefficient.

Considering a system with two ports, ports 1 and 2, the S-matrix is a 2x2 matrix :

$$\begin{pmatrix} b_1 \\ b_2 \end{pmatrix} = \begin{pmatrix} S_{11} & S_{12} \\ S_{21} & S_{22} \end{pmatrix} \begin{pmatrix} a_1 \\ a_2 \end{pmatrix} \quad (2.4)$$

where a_i is the voltage applied to port i , b_i the voltage coming out of port i .

If a voltage V is applied at port 1, then $a_1 = V$ and $a_2 = 0$ such that the S-parameters can be determined by measuring the voltage coming out of ports 1 and 2 : the reflection coefficient $b_1 = S_{11} \cdot a_1$ and the transmission from port 1 to port 2 : $b_2 = S_{21} \cdot a_2$.

2.4 Q-factor

The Q-factor represents the quality of the system, it is defined as :

$$Q = 2\pi \frac{\text{Energy stored}}{\text{Energy dissipated per cycle}} \quad (2.5)$$

For high values of the Q-factor, as in the system studied, the Q-factor is given by the following ratio :

$$Q = \frac{f_0}{\Delta f} \quad (2.6)$$

where f_0 is the resonant frequency and Δf the full bandwidth at half maximum. It can be separated into two contributions :

$$\frac{1}{Q} = \frac{1}{Q_{int}} + \frac{1}{Q_{ext}} \quad (2.7)$$

where the internal Q-factor Q_{int} characterises the quality of the internal system, i.e. the internal loss, and the external Q-factor Q_{ext} represents the loss to the outside of the system, i.e. the designed coupling to the outside.

3 Design of the cavity

3.1 Simulations

3.1.1 Cavity for the final system

First, simulations of the electric field inside the cavity are performed with Comsol [16]. The cavity is rectangular with round edges in the x direction, as shown on figure 4. It has two coaxial cables which represent port 1 and 2. The simulations are performed supposing the cavity made of a conductor with electrical conductivity $\sigma = 10^{10}$ S/m. The dimensions are chosen so that the following requirements for the different modes are fulfilled :

- Frequency of the first mode (TE 101) around 6-6.2 GHz
- Frequency of the next mode which couples to the qubit, (TE 301), between 10-11 GHz.
- Frequencies of the higher modes which couple to the qubit (modes TE 110, 501 and 111) as high as possible, as these couplings are undesired.

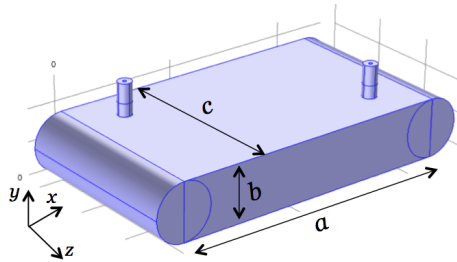


Figure 4: 3D cavity design of the Comsol simulations.

The norm of the electric field in the cavity for the first eigenmodes of the cavity are shown in figure 5. The mode TE 101, for example, has one maximum in x , no maximum in y and one maximum in z .

Possible dimensions to achieve these requirements are : $a = 44$ mm, $b = 9$ mm and $c = 28$ mm. The frequencies and quality factor of eigenmodes of the cavity are presented in table 3.1.

	Mode	Eigenfrequency [GHz]	Quality factor
1	101	6.10458	89544
2	201	7.94000	108912
3	301	10.28716	128962
4	102	11.10235	114389
5	202	12.20975	119795
8	501	15.52681	164784

Table 3.1: Frequencies and Q -factor of modes of the cavity (Simulations from COMSOL).

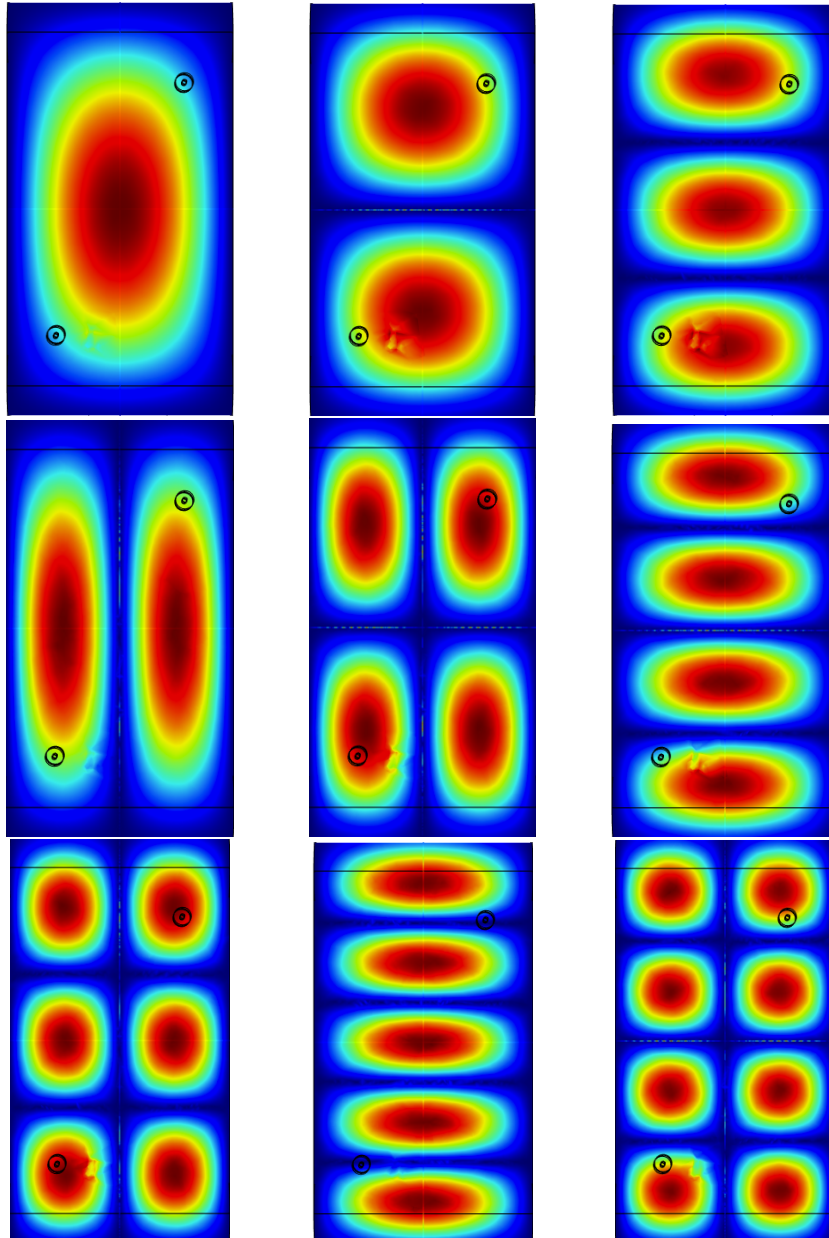


Figure 5: First cavity eigenmodes obtained with Comsol

From the quality factor Q , the factors Q_{ext} and Q_{int} can be determined by fitting S_{21} as a function of frequency, as shown in figure 6. The fitting is given by the function $L(T_0, Q, f_0, f) = \frac{T_0}{4Q^2} \frac{1}{(\frac{f}{f_0} - 1)^2 + 1/4(\frac{1}{Q})^2}$, where $T_0 = \max(S_{21})$ and f_0 is the resonant frequency.

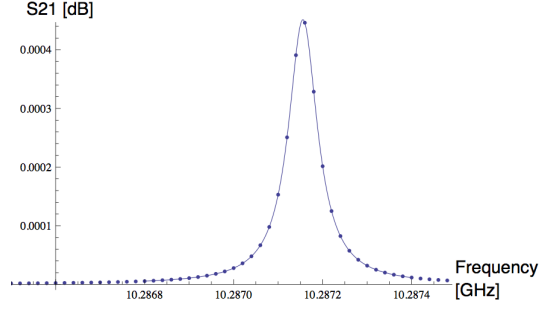


Figure 6: Lorentzian fitting of the S_{21} parameter for the mode 301, with $f_0 \simeq 10.287$ GHz

The external and internal Q-factors for the four first modes of the cavity are presented in table 3.2.

Mode	Q_{ext}	Q_{int}
101	$2.92771 \cdot 10^7$	89680
201	$8.3288 \cdot 10^6$	110365
301	$6.07742 \cdot 10^6$	131915
401	$6.50747 \cdot 10^6$	116523

Table 3.2: Expected external and internal Q-factors for the first four modes of the cavity.

3.1.2 Cavity for the study of the coupling

In order to study the coupling between the cavity and a waveguide, a cavity with different dimensions is designed. The aim is that the first two modes of the cavity which couple to the qubit, namely the TE 101 and TE 301 modes, can both couple to the waveguide. Their frequencies thus must be in the operating frequency range of the waveguide. With a cavity of dimension $a = 51$ mm, $b = 9$ mm and $c = 18$ mm, this requirement is fulfilled. The frequencies of the first five modes of this cavity are shown in table 3.3.

	Mode TE	Frequency [GHz]
1	101	8.73
2	201	9.74
3	301	11.23
4	401	13.04
5	501	15.04

Table 3.3: Expected resonance frequencies of the first five modes of the cavity.

3.2 Design and fabrication of the cavity

The design of the cavity was made using the 3D CAD software Inventor [17].

The cavity is composed of two parts : the so-called bottom part of the cavity (Figure 7, left) and the coupling plate (Figure 7, right). The drawings of these two parts are presented in the Appendix.

The coupling plate can be fixed with four screws on the cavity, with the coupling hole in the middle of the plate. The four remaining holes are for the mounting of the waveguide on the other side of the plate.

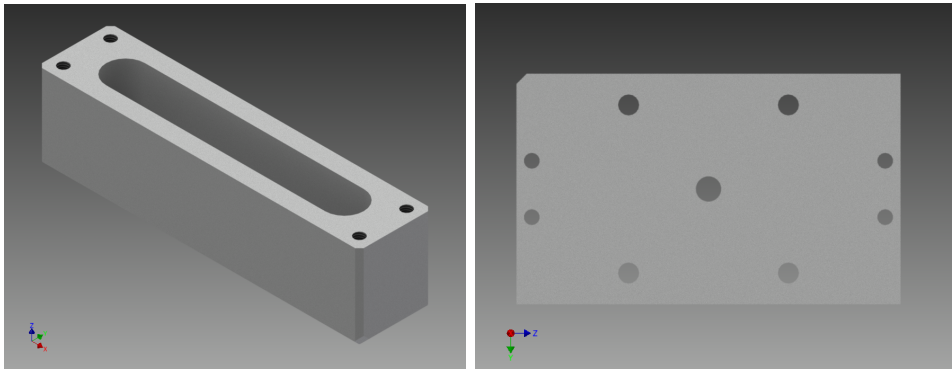


Figure 7: CAD design of the cavity.

On the left : the bottom part. On the right : the coupling plate.

The bottom part of the cavity is made of Al6061-T6 and stays the same for all the measurements. The characteristics of the coupling plate are modified in order to see the influence of several parameters on the coupling strength. The modifications on the coupling plate are :

- The radius of the coupling hole is varied from 2.5 mm to 4.5 mm ;
- The thickness of the coupling plate is between 0.8 and 2.0 mm ; and
- The aluminium purity of the material which is used for the coupling plate is either Al6061-T6 (with aluminium purity between 95.85% and 98.56%), or an Aluminium of 99.5% purity.

4 Measurements

This chapter presents the measurement setup and explains how Q_{int} and Q_{ext} are extracted from each measurement.

The first series of measurements are performed with two coupling plates of different thicknesses, both made of Al6061. For the first plate, of thickness 2.00 mm, the diameter of the hole is initially of 6 mm and is increased by steps of 1 mm until 9 mm, which is the height of the cavity. For the second plate, of thickness 1.50 mm, the diameter of the hole is varied from 4 mm to 9 mm by steps of 1 mm.

4.1 Measurement setup

To measure the cavity resonances, a reflection measurement is performed with a Virtual Network Analyzer (VNA). The power is set on -5.00 dB/m, the frequency is swept from 6 GHz to 15 GHz and the reflection parameter S_{11} is measured.

Figure 8 illustrates the measurement setup. The cavity is assembled to a waveguide which is connected to the VNA.

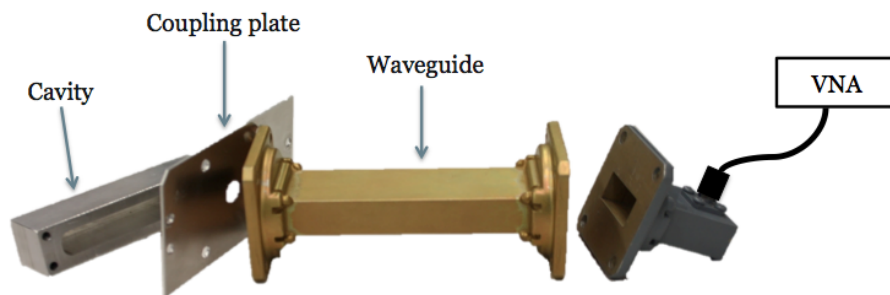


Figure 8: Scheme of the measurement setup

4.2 Calibration and background subtraction

First, the VNA is calibrated up to the waveguide.

Furthermore, a measurement of the "background" is performed, to reduce the effects of the resonances in the waveguide. Therefore, a measurement similar to the one explained above is performed, expect that the cavity is disassembled from the waveguide and only the coupling plate stays attached.

The Lorentzian model fits better the data after background subtraction. The uncertainty given by the fitting on the values of Q_{ext} and Q_{int} are lower with the resulting data, especially for small hole radius.

4.3 Measurement results

In figure 9, the real part of S_{11} is plotted as a function of the frequency. The resonant peaks on the spectrum indicating the resonance frequencies of the cavity are even more visible when the background data is subtracted from the data with the cavity, as can be seen on figure 9 (on the right).

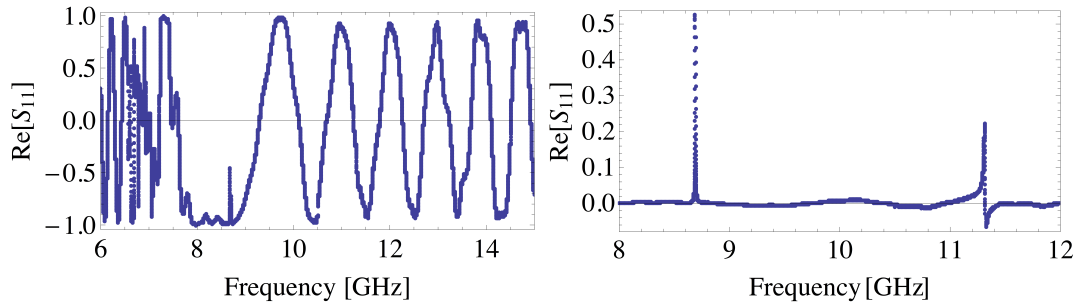


Figure 9: Spectrum [on the left] and spectrum with background subtraction [on the right] of the cavity resonances with the 1.5 mm thick plate with $r = 3.0$ mm.

A resonance can also be identified as a circle in the complex graph of S_{11} ($\text{Im}[S_{11}]$ as a function of $\text{Re}[S_{11}]$), which is shown in figure 10. The graph on the left shows the data measured with the cavity (data with background) and the data measured without the bottom part of the cavity (background). On this graph, only two circles come from the data with background but are absent from the background, these are the searched resonances of the cavity. By directly subtracting the data of the background from the original data, only these circles remain, without considering the small circles around the origin, corresponding to noise.

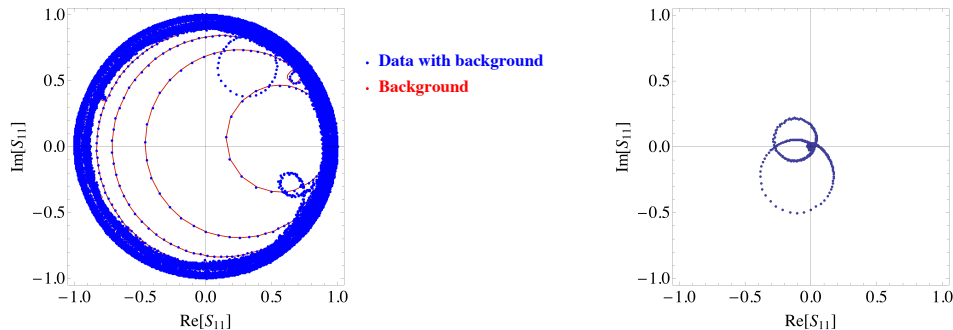


Figure 10: Measurements of S_{11} with and without background subtraction, for the 101 mode of the plate of thickness 1.5 mm and radius 3.0 mm.

4.4 Fitting of the data

The values of the external and internal Q-factors, Q_{ext} and Q_{int} , are extracted from the data by a fit of the resonances of the S parameter. Two different fitting methods were considered.

The explanation of these fittings can be found in [14] (Petersan & Anlage, 1998) and is reported here, adapted for the reflection coefficient S instead of the transmission coefficient S_{21} . The second fitting method is also explained in [15] (Kajfez, 2005).

The complex reflection coefficient S is given in the limit of weak coupling and near

resonance ($f \simeq f_0$) by :

$$S(f) = \frac{\bar{S}}{\sqrt{1 + i2Q(\frac{f}{f_0} - 1)^2}} \quad (4.8)$$

where \bar{S} is the maximum of the coefficient which occurs at the peak of the resonance ($f = f_0$).

The real and imaginary parts of S are given by the following equations :

$$\text{Re}[S(f)] = \frac{\bar{S}}{\sqrt{1 + 4Q^2(\frac{f}{f_0} - 1)^2}} \quad (4.9)$$

$$\text{Im}[S(f)] = \frac{-\bar{S}2Q(\frac{f}{f_0} - 1)}{\sqrt{1 + 4Q^2(\frac{f}{f_0} - 1)^2}} \quad (4.10)$$

The first fitting method is a simultaneous complex Lorentzian fit. As given by equations 4.9 and 4.10, $\text{Re}[S(f)]$ and $\text{Im}[S(f)]$ versus frequency data simultaneously fit a Lorentzian curve using a nonlinear least-squares fit. Figure 11 shows the result of such a fit from one of the S_{11} measurement.

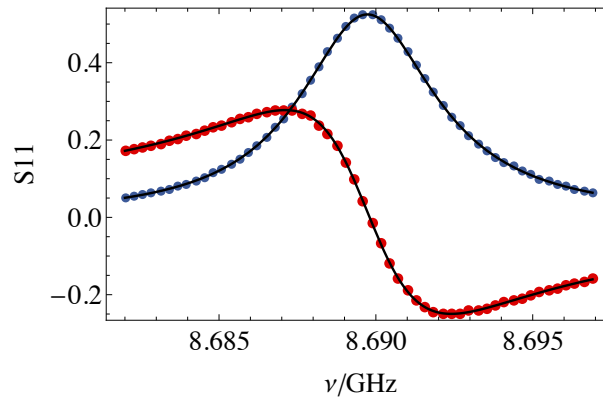


Figure 11: First fitting of the resonance of the 101 mode of the 1.5 mm thick plate with $r = 3.0$ mm. $\text{Re}[S_{11}]$ is fitted in blue and $\text{Im}[S_{11}]$ in red.

The second fitting method is called the phase versus frequency fit. It consists of two fits.

First, considering the data points near the resonance in the graph of $\text{Im}[S]$ as a function of $\text{Re}[S]$, a circle fit is made, using a linearized least-squares algorithm. Each data point is assigned a weight such that the points closer to the resonant frequency have a heavier weight than those further away. The circle fit determines the centre and radius of a circle which is a best fit to the data.

Then, the circle is rotated and translated so that its centre lies at the origin of the S plane. The intersection of the circle with the positive real axis gives an estimation of the resonant frequency. The phase angle of every data point with the positive real axis is then

calculated. Finally, the phase, $\text{Arg}(S)$, as a function of frequency is fit, using a nonlinear least-squares fit to :

$$\phi(f) = \phi_0 + 2 \tan^{-1} \left(2Q \left(1 - \frac{f}{f_0} \right) \right)$$

where ϕ_0 is the angle at which the resonant frequency occurs, f_0 and Q are determined from the fit [14].

Figure 12 presents a result of this second method of fitting.

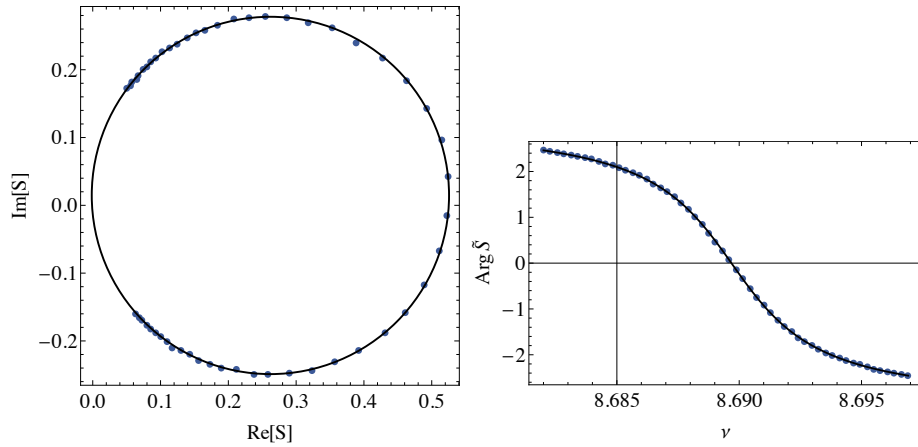


Figure 12: Second fitting of the resonance of the 101 mode of the 1.5 mm thick plate with $r = 3.0$ mm

Both fitting methods give similar results from the reflection coefficient measurements.

5 Results and discussion

5.1 Measurement results and discussion

First, the reflection coefficient is measured for two different plates of aluminium of thickness 1.5 mm and 2.0 mm, with varying radii of the coupling hole. Two resonances appear clearly after background subtraction, corresponding to the TE 101 and TE 301 modes. From the fitting of these resonances the external Q-factor Q_{ext} and the internal Q-factor Q_{int} can be extracted. For a radius of the hole below 2.5 mm, too few data points are measured at the resonances to obtain a fitting.

In figures 13 and 14, the measured values of Q_{ext} are plotted for each radius of the coupling hole and compared to the simulations. The measured values of Q_{ext} decrease as the radius of the hole increases, as predicted by the simulations.

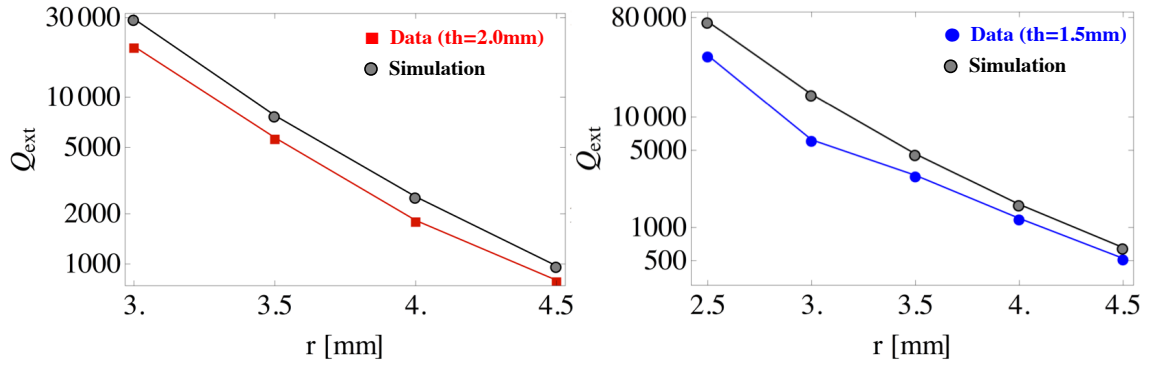


Figure 13: Measurements and simulations results of Q_{ext} as a function of the hole radius r for the 101 mode of the plates of thickness 2.0 mm [on the left] and 1.5 mm [on the right].

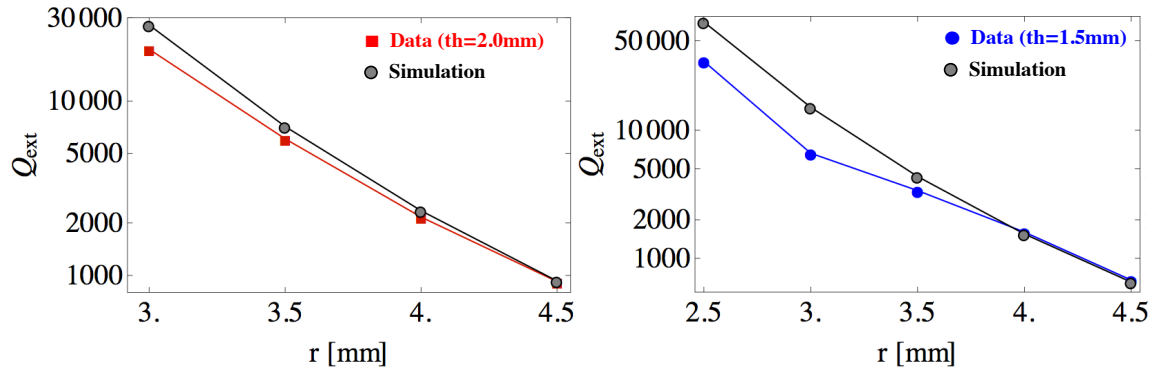


Figure 14: Measurements and simulations results of Q_{ext} as a function of the hole radius r for the 301 mode of the plates of thickness 2.0 mm [on the left] and 1.5 mm [on the right].

Comparing the results for the different plates, for a fixed hole radius, the Q_{ext} is higher for the thicker plate, as presented on figure 15.

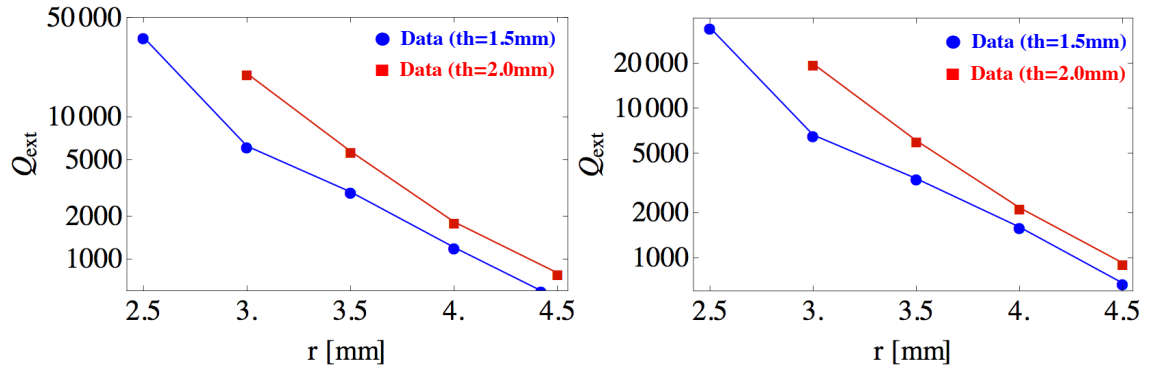


Figure 15: Comparison of the Q_{ext} measurement results as a function of the hole radius r for the two plates.

Figure 16 presents the internal Q-factor Q_{int} as a function of the radius of the coupling hole for the two plates. The Q_{int} is higher for the thinner plate, up to a hole radius of 4 mm. This is not the case anymore for the measurements with a hole radius of 4.5 mm.

The cavity height is 9 mm, hence when the radius of the coupling plate reaches $r = 4.5$ mm, the hole has the same size as the height of the cavity. If the hole is not exactly centred and aligned with the cavity, then the edges of the cavity might influence the coupling. To avoid this source of error for the next measurements, the radius is kept below 4.5 mm.

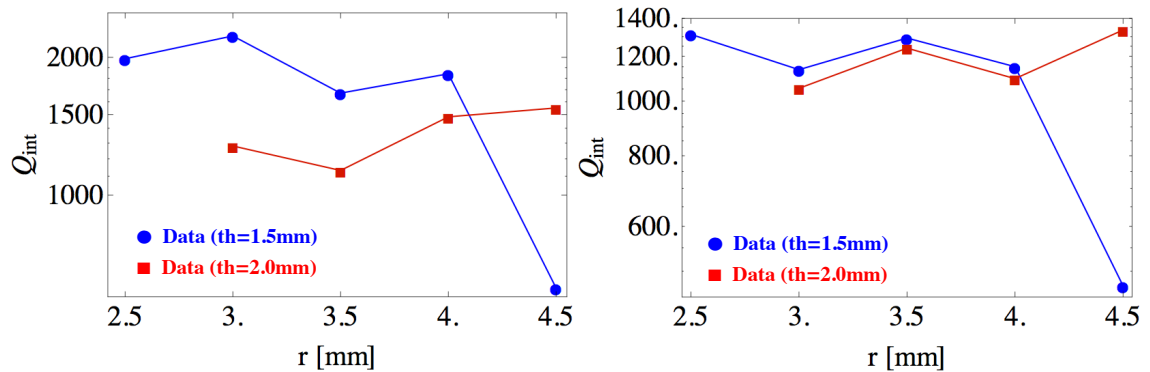


Figure 16: Comparison of the Q_{int} measurement results as a function of r for the two plates.

5.2 Simulations and sources of errors

As observed in the previous section, the measurements results are quite close to the simulations but the external Q-factor Q_{ext} is lower than expected. To understand the discrepancies between measurements and simulations, complementary simulations are made.

In the initial simulations, the cavity and the plate were supposed to be almost perfect conductors, with an electrical conductivity of 10^{10} S/m. In reality, they are made of Al6061-T6, with an electrical conductivity of $2.459 \cdot 10^7$ S/m. Simulations with a plate of lower electrical conductivity are performed, using the geometry presented in figure 17.

They result in a lower quality factor than with a perfect conductivity. Indeed, a better conductivity means less surface currents and leads to less losses.

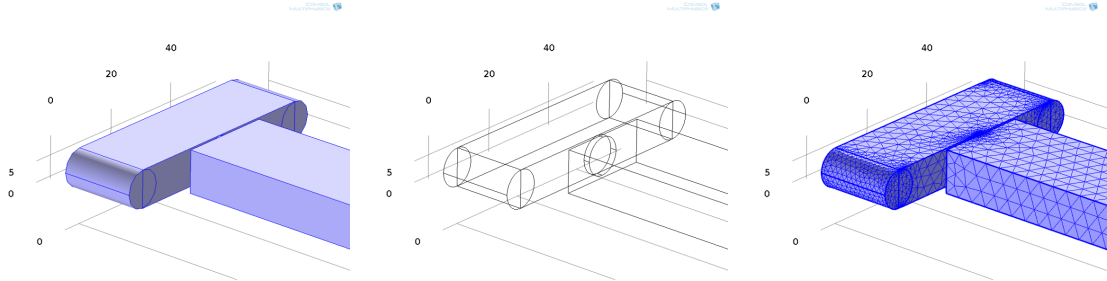


Figure 17: Geometry of the cavity, the coupling plate and the waveguide used in the COMSOL simulations.

Left : Plain objects. Middle : Lines. Right : Mesh.

Furthermore, if the contact between the plate and the cavity is not perfect, the internal Q-factor should be lower than expected. Simulations including a thin insulating layer between the bottom part of the cavity and the coupling plate are realised to study this effect.

The parameters used for the simulations are : an electrical conductivity of 10^8 S/m for the cavity and the plate and 10^{10} S/m for the waveguide. The thickness of the coupling plate is 0.8 mm and the radius of the coupling hole is 3.0 mm. The thickness of the insulating layer is fixed at 0.2 mm and its electrical conductivity is varied between 10^2 and 10^8 S/m.

A frequency sweep of the S_{11} parameter around the resonant frequency of the TE 101 mode (around 8.7 GHz) is realised, figure 18. As the electrical conductivity of the insulating layer, $\sigma_{insulator}$, increases from 100 S/m to 10^8 S/m, which equals the conductivity of the cavity, the S_{11} peak becomes sharper, corresponding to a higher Q_{ext} .

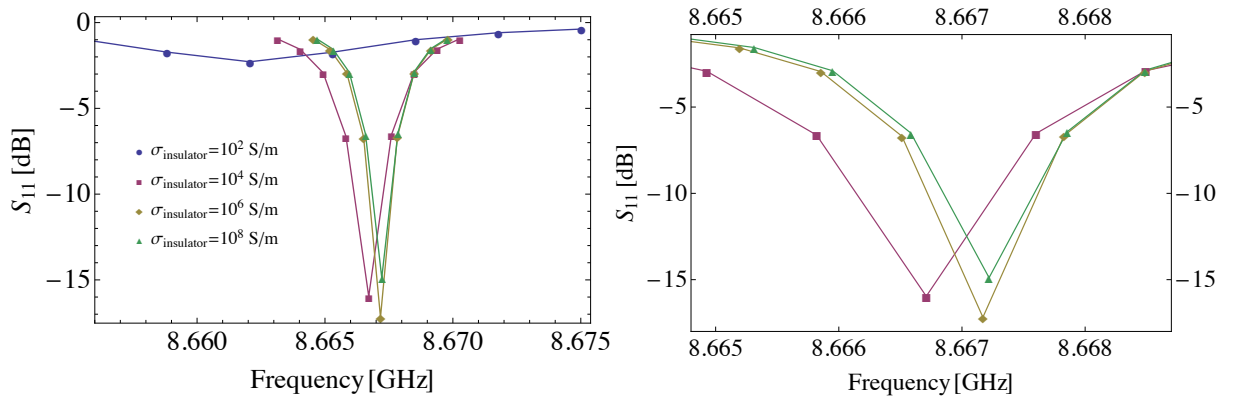


Figure 18: Frequency sweep of the S_{11} parameter around the eigenfrequency of the first mode, for different conductivity of the insulating layer.

As can be seen on figure 19, the quality factor increases as the conductivity of the insulating layer increases. The eigenfrequency of the resonance is also shifted.

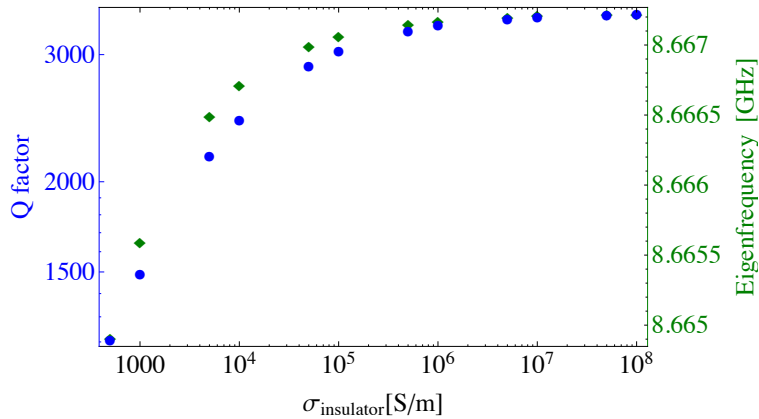


Figure 19: Log-log plot of the Q factor and the eigenfrequencies as a function of the conductivity $\sigma_{insulator}$ of the insulating layer of thickness 0.2 mm.

An important source of error in the measurement results might be that the chamfer of the hole is too big such that the measurement actually correspond to one for a hole radius slightly higher than indicated. This would mean that the results are closer to the simulations.

5.3 Measurements with high purity Aluminium

A new series of measurements is performed using plates with an Aluminium of 99.5% purity (1050A, H14). Three different plates are studied, with thicknesses 0.8 mm, 1.0 mm and 1.5 mm.

Using the same measurement setup as before, the frequency is swept from 7 GHz to 12 GHz and the S_{11} parameter is measured. Figures 20 shows a typical measurement of the data, the background, and the data with subtracted background. A spectrum of the final data is also shown in figure 21. The two resonances are clearly visible, corresponding to the TE 101 and 301 modes, as before.

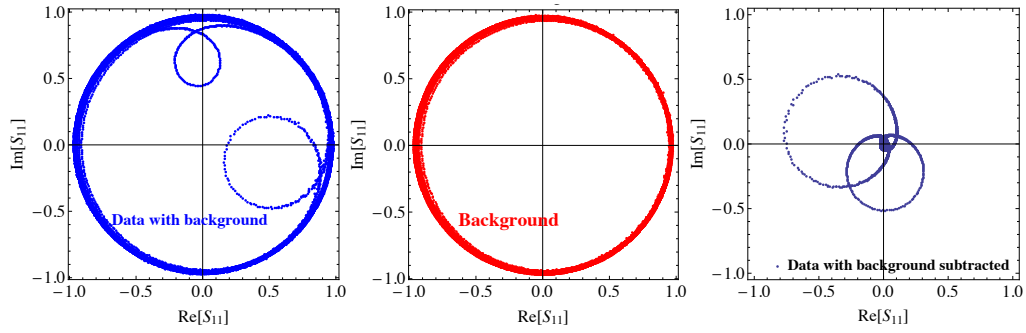


Figure 20: Data, background and data with background subtraction. Measurement with a 1.0 mm thick Al99.5 plate and a 3.5 mm hole radius.

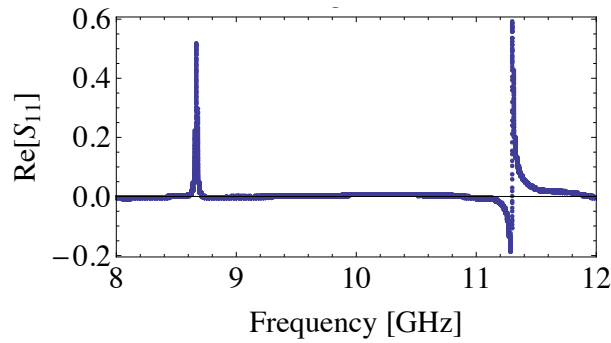


Figure 21: Spectrum with background subtraction of the cavity resonances with the 1.0 mm thick Al99.5 plate with a 3.5 mm hole radius.

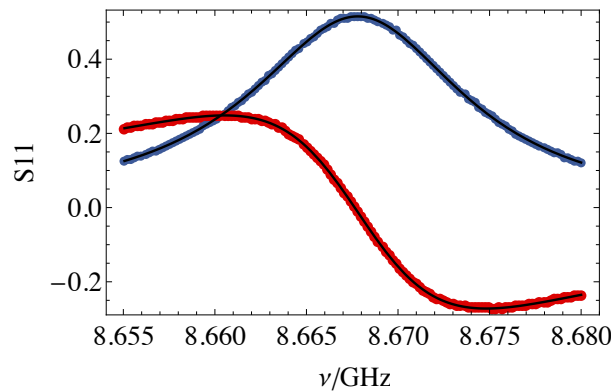


Figure 22: First fitting method of the resonance of the TE 101 mode of the 1.0 mm thick Al99.5 plate with a 3.5 mm hole radius.

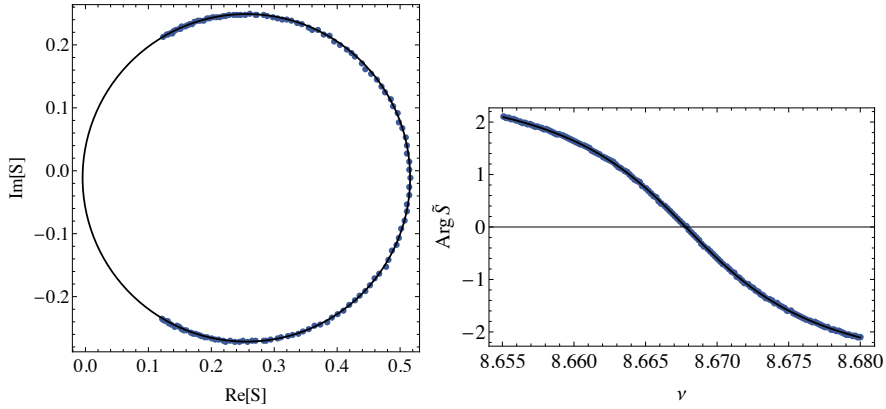


Figure 23: Second fitting method of the resonance of the TE 101 mode of the 1.0 mm thick Al99.5 plate with a 3.5 mm hole radius.

The data are much cleaner than with the previous series of measurements. This is explained by the fact that the frequency is swept only between 7 and 12 GHz instead of 6 to 15 GHz, which avoids all the noise in the lowest and highest frequency of the previous sweep.

The fittings of the datas are also more precise with both methods, see figures 22 and 23. As more data points can be used for the fitting, the values of the external and internal Q-factors are extracted from the fittings with smaller incertitude.

The external Q-factors Q_{ext} for each plate are plotted as a function of the hole radius and compared to the simulations in figures 24, 25 and 26. The measurements follow closely the simulations, for all three thicknesses and for the two modes.

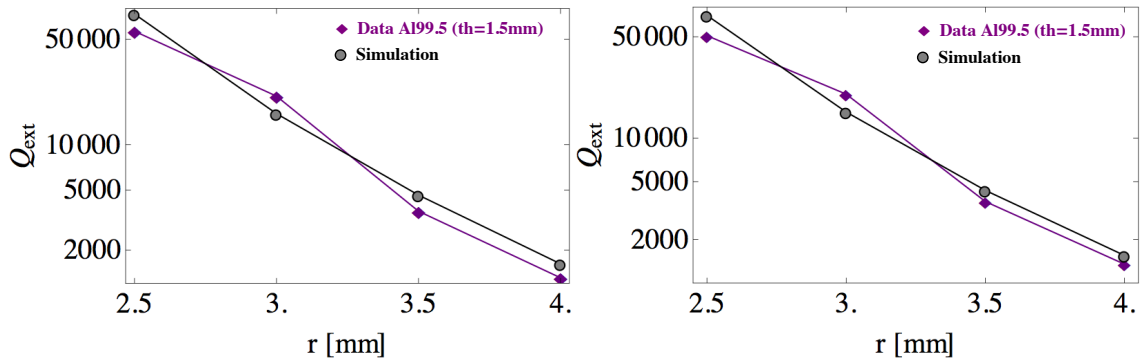


Figure 24: Measurements and simulations results of Q_{ext} as a function of the hole radius r of the 1.5 mm thick Al99.5 plate, for the 101 mode [on the left] and the 301 mode [on the right].

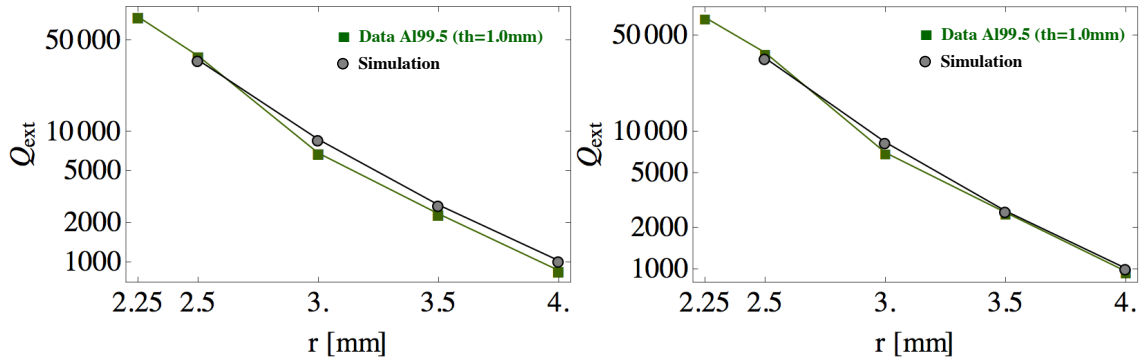


Figure 25: Measurements and simulations results of Q_{ext} as a function of the hole radius r of the 1.0 mm thick Al99.5 plate, for the 101 mode [on the left] and the 301 mode [on the right].

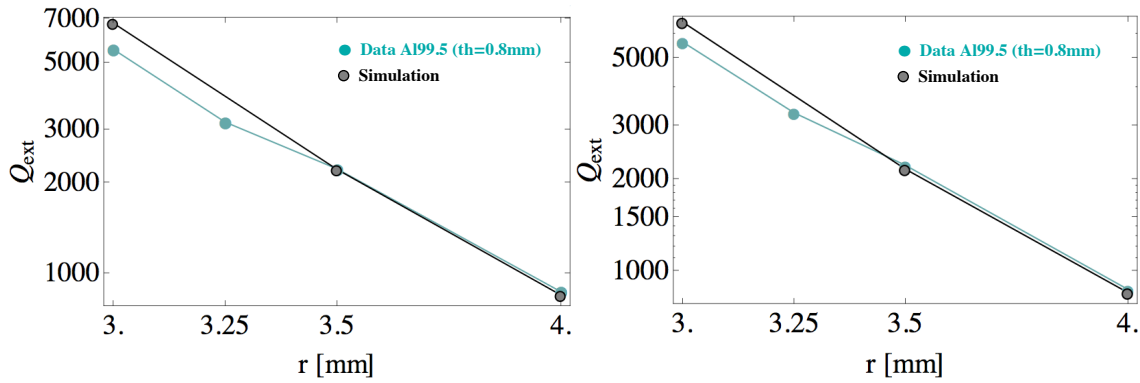


Figure 26: Measurements and simulations results of Q_{ext} as a function of the hole radius r of the 0.8 mm thick Al99.5 plate, for the 101 mode [on the left] and the 301 mode [on the right].

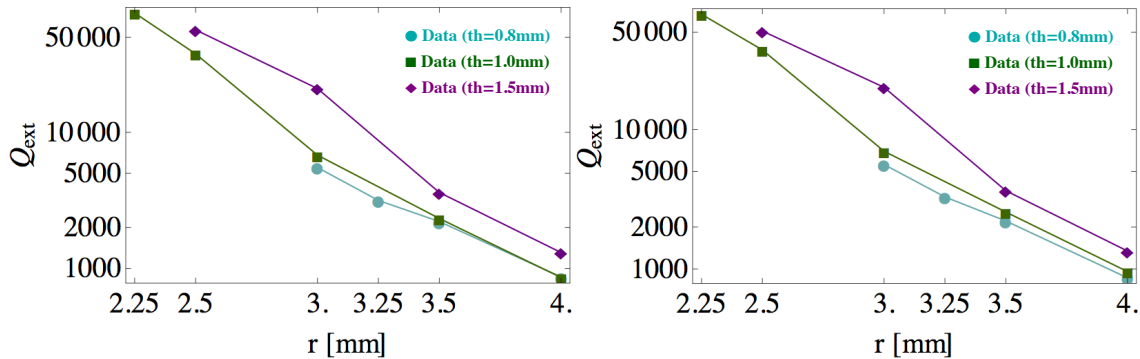


Figure 27: Comparison of the measurement results of Q_{ext} as a function of the hole radius r of Al99.5 plates of three thicknesses, for the 101 mode [on the left] and the 301 mode [on the right].

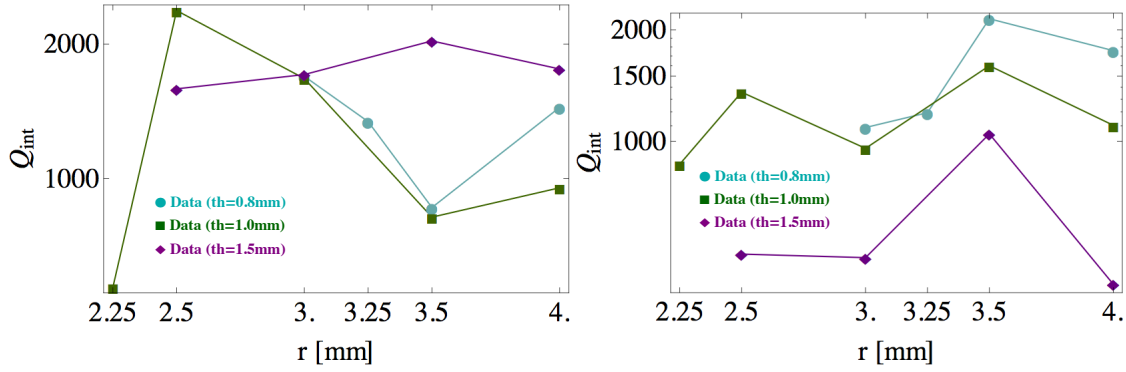


Figure 28: Comparison of the measurement results of Q_{int} as a function of the hole radius r of Al99.5 plates of three thicknesses for the 101 mode [on the left] and the 301 mode [on the right].

Figure 27 presents a comparison of Q_{ext} as a function of the hole radius for the three different plate thicknesses. As observed with the first series of measurements, the thicker the coupling plate, the higher the Q_{ext} , for each hole radius. This is valid for the two modes investigated.

The higher material purity of the plate from the second series of measurement is expected to lead to better Q_{ext} and Q_{int} values. By comparing the Q_{ext} of the plates of different types of Aluminium (figure 29), it appears that the Q_{ext} of the plate made of Al99.5% is almost always higher than the other plate made of lower purity aluminium, and therefore closer to the values of the simulations. The label 'Data' refers to the first series of measurements with the lower purity aluminium and the label 'Data Al99.5' refers to the measurements of the 99.5% purity aluminium.

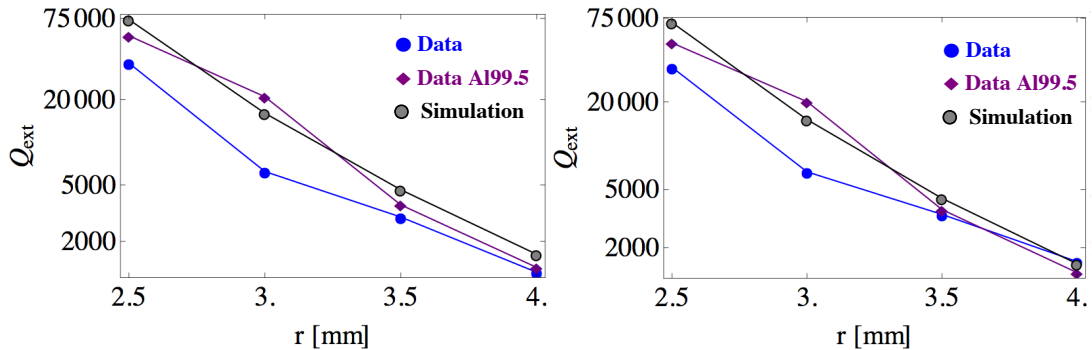


Figure 29: Comparison of the measurements results of Q_{ext} as a function of the hole radius r for two different plates of different material and same thickness, for the 101 mode [on the left] and the 301 mode [on the right].

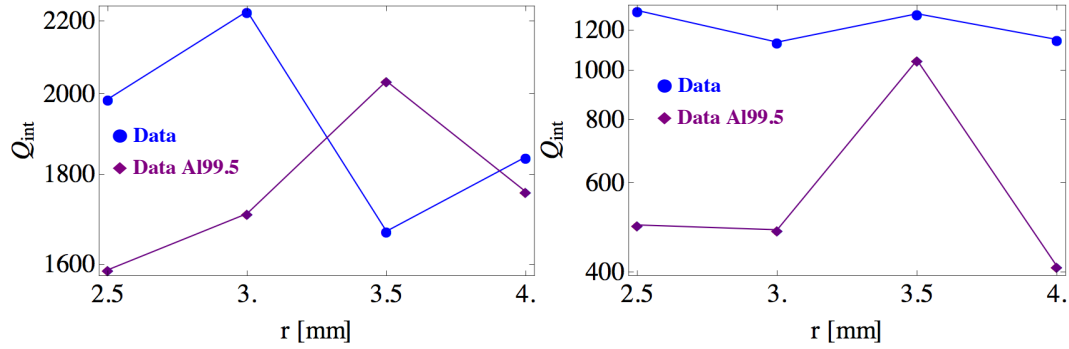


Figure 30: Comparison of the measurement results of Q_{int} as a function of the hole radius r for two different plates of different material and same thickness, for the 101 mode [on the left] and the 301 mode [on the right].

By using a plate made of a purer material, the reflection measurements are less noisy, and the measurement data are closer to the simulated values. This leads to believe that using a higher quality plate, the systematic error in the measurements is diminished. Thus using a good material is important to get precise and exact measurement results.

6 Conclusion

The design and fabrication of a system composed of a 3D microwave cavity coupled to a waveguide was realised.

The dimensions of the cavity can tune the eigenfrequencies of the eigenmodes of the cavity. These simulations allowed to choose the optimal dimensions to fulfil specific requirements on the different modes inside the cavity. These dimensions were thus chosen so that only the first two modes coupling to the qubit placed in the middle of the cavity, i.e. the modes TE 101 and TE 301, will propagate into the waveguide. Their frequencies are in the optimal usable frequency range of the waveguide WR90.

A coupling plate with a hole in the middle assures the coupling between the waveguide and the cavity. By adjusting two parameters of the geometry of the plate, namely the thickness of the plate and the radius of the coupling hole, one can obtain the desired external Q-factor, and the corresponding internal Q-factor.

The quality of the material used has also an importance in the quality factor of the system. To obtain better results, the conductivity of the cavity and the plate should both be of high value.

In conclusion, the expected resonance frequencies of each mode, depending on the dimensions of the cavity, can be determined by simulations and correspond closely to the measured resonance frequencies. For a specific thickness of the coupling plate and hole radius, the internal and external Q-factors determined by a reflection measurement and fitting of the resulting resonance peaks also follow closely the simulations.

7 Acknowledgment

This work was the continuation of a semester thesis by Silvia Ruffieux, supervised by Philipp Kurpiers, called 'Simulation and characterisation of waveguide and the coupling to 3D microwave cavities'. In particular, the simulations in COMSOL were adapted from existing simulations of a previous version of the cavity.

Philipp Kurpiers is the supervisor of this semester thesis. He is at the origin of this project and he was crucial to the realisation of this thesis. His explanations and availability were greatly appreciated and I really enjoyed working with him.

I would like to thank Prof. Andreas Wallraff for offering me the possibility to do my semester thesis in the Quantum Device Lab. I really enjoyed working in the lab and hope I made a positive contribution to its research.

References

- [1] A. Einstein, B. Podolsky & N. Rosen, Phys. Rev. 47, 777 (1935).
- [2] J.S. Bell, Physics (Long Island City, N.Y.) 1, 195 (1965).
- [3] J. F. Clauser, M. A. Horne, A. Shimony & R. A. Holt, Phys. Rev. Lett. 23, 880 (1969).
- [4] S. J. Freedman & J. F. Clauser, Phys. Rev. Lett. 28, 938 (1972).
- [5] A. Aspect, P. Grangier & G. Roger, Phys. Rev. Lett. 47, 460 (1981).
- [6] A. Aspect, P. Grangier & G. Roger, Phys. Rev. Lett. 49, 91 (1982).
- [7] M. A. Rowe, D. Kielpinski, V. Meyer, C. A. Sackett, W. M. Itano, C. Monroe & D. J. Wineland, Nature (London) 409, 791 (2001)
- [8] G. Weihs, T. Jennewein, C. Simon, H. Weinfurter & A. Zeilinger, Phys. Rev. Lett. 81, 5039 (1998).
- [9] D. N. Matsukevich, P. Maunz, D. L. Moehring, S. Olmschenk & C. Monroe, Phys. Rev. Lett. 100, 150404 (2008)
- [10] M. Ansmann, H. Wang, R. C. Bialczak, M. Hofheinz, E. Lucero, M. Neeley, A. D. O'Connell, D. Sank, M. Weides, J. Wenner, A. N. Cleland & J. M. Martinis, Nature 461, 504 (2009).
- [11] M. Giustina, A. Mech, S. Ramelow, B. Wittmann, J. Kofler, J. Beyer, A. Lita, B. Calkins, T. Gerrits, S. W. Nam, R. Ursin & A. Zeilinger, Nature 497, 227 (2013).
- [12] David M. Pozar, *Microwave Engineering*, University of Massachusetts at Amherst, 4th edition, 2011.
- [13] <http://microwaves101.com/encyclopedia/waveguideloss.cfm>
- [14] Paul J. Petersan & Steven M. Anlage, *Measurement of resonant frequency and quality factor of microwave resonators: Comparison of methods*, J. Appl. Phys. 84, 3392 (1998)
- [15] Darko Kajfez, *Q-Factor* in «Encyclopedia of RF and Microwave Engineering», University of Mississippi, 2005
- [16] Comsol Multiphysics®, COMSOL, <http://www.comsol.com>
- [17] Inventor®, 3D CAD software for mechanical design, Autodesk, <http://www.autodesk.com>

Appendix

2D plans from Autodesk inventor

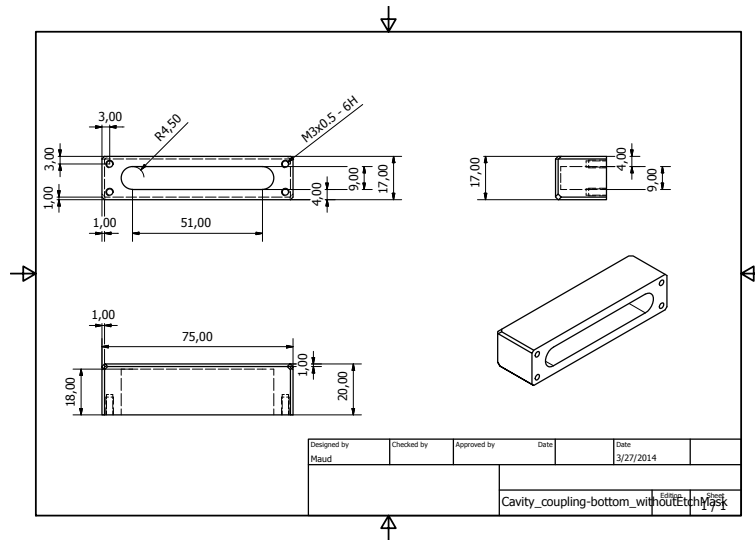


Figure 31: Drawing of the bottom part of the cavity

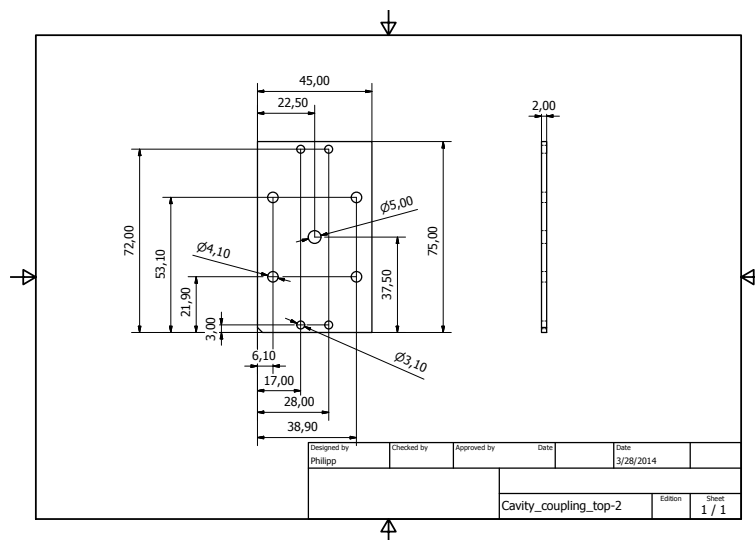


Figure 32: Drawing of the plate



Eidgenössische Technische Hochschule Zürich
Swiss Federal Institute of Technology Zurich

Declaration of originality

The signed declaration of originality is a component of every semester paper, Bachelor's thesis, Master's thesis and any other degree paper undertaken during the course of studies, including the respective electronic versions.

Lecturers may also require a declaration of originality for other written papers compiled for their courses.

I hereby confirm that I am the sole author of the written work here enclosed and that I have compiled it in my own words. Parts excepted are corrections of form and content by the supervisor.

Title of work (in block letters):

Design and coupling of a 3D microwave cavity
to a waveguide.

Authored by (in block letters): Maud Barthélemy
For papers written by groups the names of all authors are required.

Name(s):

First name(s):

With my signature I confirm that

- I have committed none of the forms of plagiarism described in the '[Citation etiquette](#)' information sheet.
- I have documented all methods, data and processes truthfully.
- I have not manipulated any data.
- I have mentioned all persons who were significant facilitators of the work.

I am aware that the work may be screened electronically for plagiarism.

Place, date

Bristol, 29.09.2014

Signature(s)

M. Barthélemy

For papers written by groups the names of all authors are required. Their signatures collectively guarantee the entire content of the written paper.